

See discussions, stats, and author profiles for this publication at: <https://www.researchgate.net/publication/366635249>

Multi-proxy evidence for rapidly shifting sediment sources to the Taiwan Western Foreland Basin at the Miocene–Pliocene transition

Article in *Basin Research* · December 2022

DOI: 10.1111/bre.12741

CITATIONS

3

READS

111

8 authors, including:



Amy Hsieh

Simon Fraser University

16 PUBLICATIONS 142 CITATIONS

[SEE PROFILE](#)



Shahin E. Dashtgard

Simon Fraser University

120 PUBLICATIONS 3,209 CITATIONS

[SEE PROFILE](#)



Pei-Ling Wang

National Taiwan University

124 PUBLICATIONS 2,883 CITATIONS

[SEE PROFILE](#)



Chong-Shern Horng

Academia Sinica

84 PUBLICATIONS 3,244 CITATIONS

[SEE PROFILE](#)

Multi-proxy evidence for rapidly shifting sediment sources to the Taiwan Western Foreland Basin at the Miocene–Pliocene transition

Amy I. Hsieh^{1,2}  | Shahin E. Dashtgard¹  | Pei-Ling Wang^{3,4} |
 Chorng-Shern Horng⁵  | Chih-Chieh Su^{3,4}  | Andrew T. Lin⁶  |
 Romain Vaucher⁷  | Ludvig Löwemark^{2,4} 

¹Paleoclimate Records in Shallow Marine Strata (PRISMS) Research Group, Department of Earth Sciences, Simon Fraser University, Burnaby, Canada

²Department of Geosciences, National Taiwan University, Taipei, Taiwan

³Institute of Oceanography, National Taiwan University, Taipei, Taiwan

⁴Research Center for Future Earth, National Taiwan University, Taipei, Taiwan

⁵Institute of Earth Sciences, Academia Sinica, Taipei, Taiwan

⁶Department of Earth Sciences, National Central University, Taoyuan, Taiwan

⁷Institute of Earth Sciences, University of Lausanne, Lausanne, Switzerland

Correspondence

Amy I. Hsieh, Paleoclimate Records in Shallow Marine Strata (PRISMS) Research Group, Department of Earth Sciences, Simon Fraser University, Burnaby, Canada.
 Email: amy_hsieh@sfu.ca

Funding information

Ministry of Education, Taiwan; Ministry of Science and Technology, Taiwan, Grant/Award Number: MOST 107-2116-M-002-011; Natural Sciences and Engineering Research Council of Canada, Grant/Award Number: RGPIN-2019-04528

Abstract

The Taiwan Western Foreland Basin is thought traditionally to have received sediment mainly from Eurasia until the late Pliocene–early Pleistocene, after which time, the Taiwan orogen became the dominant source. However, a combination of clay mineralogy, $\delta^{13}\text{C}_{\text{org}}$ and C/N of organic matter, and mass-specific magnetic susceptibility of late Miocene to early Pliocene strata of the Kueichulin Formation indicate that onset of major sediment contributions from Taiwan occurred much earlier, and correlates closely to the uplift and initial emergence of the Taiwan orogen. Clay mineralogy shows an upsection increase in illite and illite crystallinity, and a decrease in chlorite and kaolinite after the late Miocene, and this is attributed to rapid erosion of the Taiwan orogen. Results from $\delta^{13}\text{C}_{\text{org}}$ and C/N analyses show that organic material in the Kueichulin Formation changed from dominantly marine to dominantly terrestrial in the early Pliocene, and this is linked to the delivery of large quantities of terrestrial organic material from the Taiwan orogen to the adjacent Taiwan Strait. Magnetic susceptibility also decreases significantly during the early Pliocene, resulting from dilution of magnetic minerals through the influx of non-magnetic minerals delivered from the Taiwan orogenic belt. The establishment of the growing Taiwan orogen as a major sediment source to the Western Foreland Basin occurred at the Miocene–Pliocene transition, about two million years earlier than previously recognized.

KEYWORDS

clay mineralogy, denudation, foreland basin, magnetic susceptibility, organic carbon geochemistry, source-to-sink, Taiwan

1 | INTRODUCTION

1.1 | Foreland basins

Foreland basins are regions of sediment accumulation adjacent to orogenic belts, and these basins form through downward flexure of the lithosphere below the orogen (DeCelles & Giles, 1996). Foreland basins are filled by detritus that originates mainly from erosion of the adjacent orogen. Stratigraphic and facies analyses of foreland basins can be used to reconstruct the evolution of both the orogen and the basin (Covey, 1986; DeCelles & Giles, 1996; Flemings & Jordan, 1989); however, this requires an understanding of erosional and depositional processes that occurred therein.

The Taiwan orogenic belt continues to actively uplift, such that present-day orogenic and sedimentation processes can be used as an analogue for both the evolution of the adjacent Western Foreland Basin (WFB) and the mountain-building events that formed it (Covey, 1986). Early emergence of the Taiwan orogen should be recorded in the sedimentary fill of the adjacent WFB. Herein, we use clay mineralogy, $\delta^{13}\text{C}_{\text{org}}$ and C/N of organic material and mass-specific magnetic susceptibility of the late Miocene to early Pliocene Kueichulin Formation as proxies to test the timing of major sediment delivery from Taiwan to the WFB. We then discuss the implications of these data for resolving depositional controls on sedimentation.

1.2 | Previous work

Seismic reflection profiles and well data through the late Miocene to Recent strata in Taiwan reveal a wedge-shaped sedimentary succession that decreases in thickness towards the west and becomes increasingly sand-rich towards the east (Lin et al., 2003). The westward thinning of the sedimentary succession and corresponding decrease in sand content suggests that an eastern sediment source to the WFB may have dominated deposition since the late Miocene, and through the emergence and growth of the Taiwan orogen (ca. 6.5 Ma; Lin et al., 2003).

In the WFB, multiple studies have assessed changes in the composition of late Miocene to Recent sedimentary strata to infer source areas and resolve the tectonic history and evolution of the Taiwan orogen. Previous studies have suggested that Taiwan became the main sediment source to the WFB by the early Pleistocene and possibly the late Pliocene (e.g. Chamley et al., 1993; Chang & Chi, 1983; Chen et al., 1992, 2000; Chou, 1972; Covey, 1986; Dashtgard et al., 2021; Horng et al., 2012; Nagel et al., 2013, 2014, 2018; Teng, 1990). Sedimentary facies analysis of late Miocene to early Pliocene strata of

Highlights

- Multi-proxy approach to determining sediment sources to the Taiwan Western Foreland Basin.
- Variations in clay mineralogy reflect rapid erosion of the Taiwan orogen after the late Miocene.
- Changes in $\delta^{13}\text{C}_{\text{org}}$ and C/N are linked to the delivery of terrestrial organic matter eroded from the Taiwan orogen.
- Decrease in magnetic susceptibility resulted from an influx of non-magnetic minerals eroded from the Taiwan orogen.
- Results indicate Taiwan became dominant sediment source at the Miocene-Pliocene transition.

the Kueichulin Formation in northwest Taiwan indicates that the strata were deposited in 10–35 m water depths, which increased generally towards the south (Figure 1; Castellort et al., 2011; Dashtgard et al., 2020, 2021; Lin et al., 2003; Nagel et al., 2013, 2018; Shaw, 1996). Multiple directions of shallowing towards the west, north and east suggest that sediment comprising the Kueichulin Formation was derived from multiple sources, including the South China Block to the west and northwest and potentially the newly emergent Taiwan orogen to the northeast and east (Chang & Chi, 1983; Covey, 1986; Dashtgard et al., 2020; Nagel et al., 2013; Shaw, 1996). Assessments of $\delta^{13}\text{C}_{\text{org}}$ and C/N of organic material further support multiple sediment sources (Dashtgard et al., 2021), and sandstone petrography shows an increase in sedimentary lithic fragments through the Plio-Pleistocene record as a result of recycling of older foreland sedimentary deposits (Chen et al., 1992, 2000; Chen, Lee, et al., 2019; Nagel et al., 2014). In contrast to the Plio-Pleistocene record in the WFB, Nagel et al. (2014) showed that the sandstone petrography for the eastern retro-foreland basin of Taiwan (i.e. Coastal Range, Figure 2a) is characterized by an increase in metamorphic lithic fragments, which corresponds to progressive unroofing of deeper, higher grade metamorphic rocks that were exhumed through continued uplift of the Taiwan orogen. The difference in sandstone petrography between the western and eastern basins of Taiwan is attributed to the asymmetric development of the Taiwan orogen (Nagel et al., 2014).

Previous studies of clay mineralogy have shown that in the eastern retro-foreland basin of Taiwan, illite crystallinity increases with time, reflecting the progressive unroofing of the metasedimentary core of Taiwan (Nagel et al., 2014). In the WFB, illite crystallinity shows neither an increasing nor decreasing trend (Chamley et al., 1993; Chen et al., 2000;

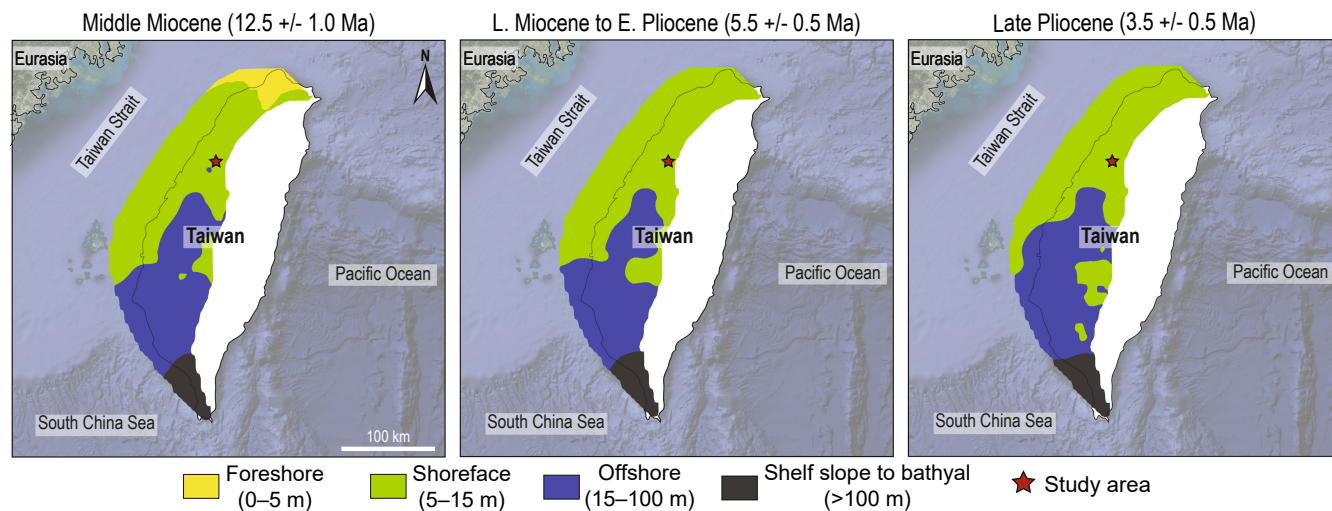


FIGURE 1 Palaeogeographic reconstructions and palaeo-water depth estimates for the Western Foreland Basin, Taiwan. The facies transitions indicate overall deepening to the south. The red star marks the location of the studied outcrop section, and numbers in meters denote estimated water depths in meters. Data and reconstructions are modified after Nagel et al. (2013).

Huang et al., 2012; Nagel et al., 2014). More specifically, in the southern WFB, illite crystallinity shows no change upwards, while in the north, there is a slight increasing trend in sediment younger than 3.5 Ma (Nagel et al., 2014). The increasing illite crystallinity in younger sediment in the northern WFB records the relatively constant rate of unroofing of the Taiwan orogen, while relatively constant illite crystallinity observed in the south is attributed to recycling of older foreland basin sediment (Nagel et al., 2014). Of note, however, the trends in illite crystallinity reported in previous studies are based on low sample densities that may not be sufficient to capture variations in the sedimentary record that reflect evolution of the basin.

Sediment discharged from modern rivers in Taiwan contains immature clay minerals with high illite and chlorite content and low smectite and kaolinite (e.g. Chen et al., 1992; Liu, Tuo, et al., 2008; Li et al., 2012). The immature clay mineralogy is a product of the rapid physical weathering of source terrains across Taiwan as a result of its steep topography, frequent earthquakes and associated landslides and tropical cyclones and high precipitation (Chen et al., 2017, 2018; Dashtgard et al., 2020; Kelman, 2013; Li et al., 2012; Milliman et al., 2017). By contrast, rivers draining the Eurasian continent deliver intermediate to mature clay minerals, such as kaolinite and smectite (Chen et al., 2017; Li et al., 2012; Liu, Liu, et al., 2008; Zhao, Zou, Gao, et al., 2018; Zhao, Zou, Liu, et al., 2018).

Analyses of $\delta^{13}\text{C}_{\text{org}}$ and C/N of particulate organic material can be used to distinguish between marine and terrestrial sourced organics (Chmura & Aharon, 1995; Czarnecki et al., 2014; Dashtgard et al., 2021; Hilton et al., 2010; Kao et al., 2014; Kao & Liu, 2000; Peterson & Fry, 1987). Marine organic matter includes marine

plankton ($\delta^{13}\text{C}_{\text{org}}$: $-20.4\text{‰} \pm 1.4\text{‰}$, C/N: 6.2 ± 1.0), marine particulate matter ($\delta^{13}\text{C}_{\text{org}}$: $-22.5\text{‰} \pm 1.7\text{‰}$, C/N: 6.2 ± 1.0) and dissolved organic matter ($\delta^{13}\text{C}_{\text{org}}$: $-22.5\text{‰} \pm 0.8\text{‰}$, C/N: 6.2 ± 1.0) (Dashtgard et al., 2021; Martiny et al., 2013). Marine plankton and particulate matter settle on the seafloor mainly under fair-weather conditions, and are incorporated into the sediment (Dashtgard et al., 2021). Terrestrial organic material includes C3 plants ($\delta^{13}\text{C}_{\text{org}}$: $-27.4\text{‰} \pm 1.9\text{‰}$, C/N: 52 ± 14.8), C4 plants ($\delta^{13}\text{C}_{\text{org}}$: $-13.2\text{‰} \pm 1.9\text{‰}$, C/N: 83.3 ± 54) and soil ($\delta^{13}\text{C}_{\text{org}}$: $-25.9\text{‰} \pm 1.2\text{‰}$, C/N: 17.1 ± 7.3) (Dashtgard et al., 2021).

Mass-specific magnetic susceptibility (χ) measures the magnetic mineral concentrations in rock, and is used to detect changes in sediment source (Thompson & Oldfield, 1986). In particular, variations in χ can be tied to changes in sedimentation processes (e.g. erosion, transport and deposition), and by extension, sedimentary environments (Hatfield, 2014; Kodama & Hinnov, 2015; Thompson & Oldfield, 1986). In the Taiwan Strait, sediment sourced from western Taiwan have χ values that range from 0.9 ± 0.3 to $1.8 \pm 0.5 \times 10^{-7} \text{ m}^3 \text{ kg}^{-1}$. Sediment sourced from the South China Block have higher values that average $4.0 \pm 1.3 \times 10^{-7} \text{ m}^3 \text{ kg}^{-1}$ (Horng & Huh, 2011). This indicates that sediment from Taiwan contains much lower concentrations of magnetic minerals compared to sediment sourced from nearby Eurasia.

1.3 | Geological background and study area

Taiwan is located at the collision zone between the Luzon Arc on the Philippine Sea Plate and the Eurasian

Plate. Collision of the two plates commenced in the late Miocene (ca. 6.5 Ma) and formed the 330 km long, 100 km wide orogenic belt that comprises the majority of Taiwan. The orogenic belt continues to uplift at a rate of approximately 5–7 mm year⁻¹ (Figure 2a; Castellort et al., 2011; Covey, 1986; Lin et al., 2003; Lin & Watts, 2002; Nagel et al., 2018; Pan et al., 2015).

The onset of collision between the Eurasian Plate and Philippine Sea Plate triggered lithospheric flexure of the Eurasian Plate, resulting in the formation of the WFB (Castellort et al., 2011; Chou & Yu, 2002; Lin & Watts, 2002; Yu & Chou, 2001). The WFB is characterized by both high-accommodation and high-sedimentation rates; sediment accumulation rates exceeded 400 m per million years in the early to mid-Pliocene and 1000 m per million years in the late Pleistocene (Chang & Chi, 1983; Chen et al., 1992; Covey, 1986; Simoes & Avouac, 2006; Vaucher et al., 2021). Late Miocene to Pliocene sedimentary strata of the Kueichulin Formation were deposited in the WFB during the early stages of the collision (Lin et al., 2003; Yu & Chou, 2001) and in mainly shallow-marine environments (Castellort et al., 2011; Covey, 1986; Dashtgard et al., 2020, 2021; Nagel et al., 2013; Pan et al., 2015). The Kueichulin Formation overlies the Nanchuang Formation and grades both upwards and southwards into the Chinshui Shale (Figure 3; Castellort et al., 2011). The

Kueichulin Formation is up to 800 m thick and consists of three members, including (from base to top): Kuantaoshan Sandstone, Shihliufen Shale and Yutengping Sandstone (Figure 3; Castellort et al., 2011; Lin et al., 2007; Pan et al., 2015; Shaw, 1996). The Kuantaoshan Sandstone consists of hummocky cross-stratified sandstone with low bioturbation intensities and scour-and-fill structures (Nagel et al., 2013). The Shihliufen Shale comprises mudstone deposited in a fully marine environment (Castellort et al., 2011; Chang, 1971; Dashtgard et al., 2021; Nagel et al., 2013) and the Yutengping Sandstone comprises sandy mudstone, muddy sandstone and sandstone with varying intensities of bioturbation (Castellort et al., 2011; Dashtgard et al., 2020, 2021; Lin et al., 2007; Nagel et al., 2013).

Nannofossil biostratigraphy indicates that the Kuantaoshan Sandstone was deposited between NN11 and NN12 based on the presence of *D. quinqueramus* and *D. berggrenii* (Figure 3; Chang & Chi, 1983; Huang, 1976; Martini, 1971; Shea & Huang, 2003). The base of the Shihliufen Shale occurs just above the middle of NN12 based on the last occurrence of *D. quinqueramus* in the Kuantaoshan Sandstone (Figure 3; Huang, 1976; Martini, 1971). Raffi et al. (2006) define the absolute age range of NN12 as 5.59–5.12 Ma, and this suggests that the boundary between the Kuantaoshan

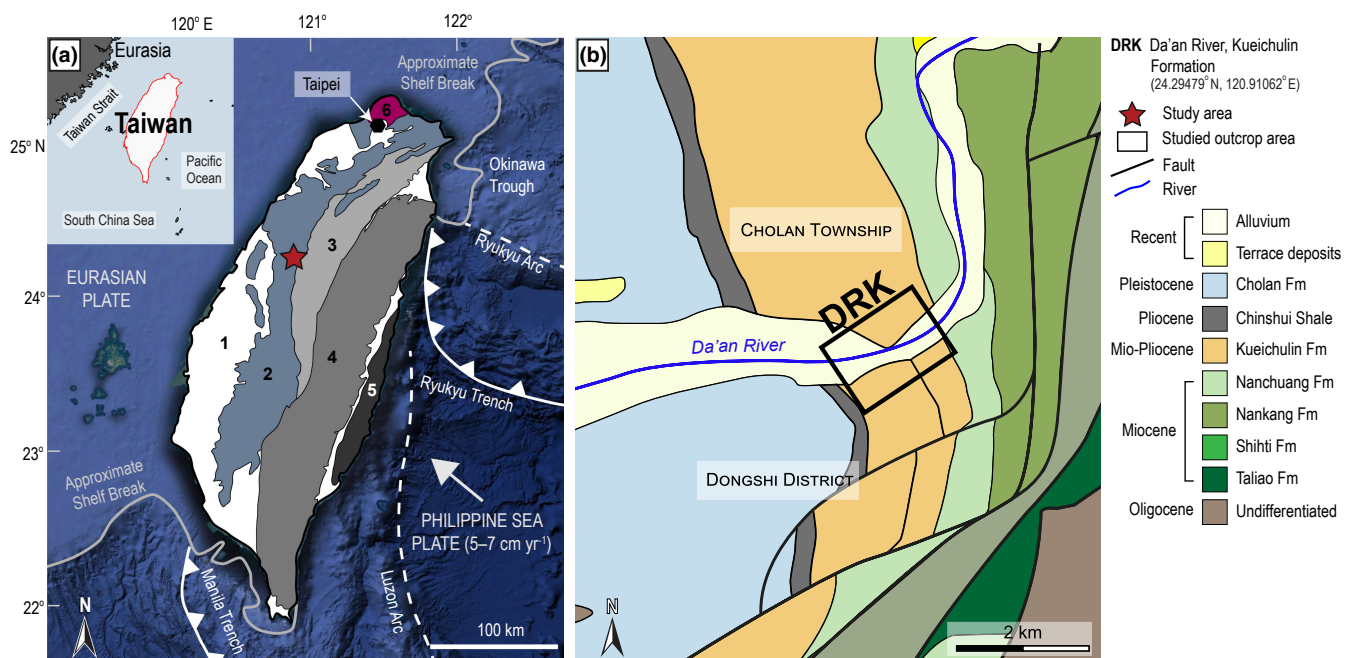


FIGURE 2 (a) Simplified geological map of Taiwan, showing the relative translation rate of the Philippine Sea Plate with respect to the Eurasian Plate. The main geological units are as follows: Coastal Plain and Terraces (1), Western Foothills (2), Hsueshan Range (3), Central Range (4), Coastal Range (5) and Tatun Volcano Group (6) (data from Lin et al. (2003), Simoes and Avouac (2006) and Lin and Chen (2016)). The inset map shows the geographical location of Taiwan, and the red star denotes the study area shown in (b). Bathymetry around Taiwan sourced from MOEA, 2019 and is modified based on formations shown in Lin and Chen (2016) and Teng et al. (1991).

Age (Ma)	Period	Epoch	Western Foothills		Nannofossil Zonations
			North-Central		
0.77	QUATERNARY	PLEISTOCENE	Toukoshan Fm		NN19
1.80			Cholan Fm		
2.58	NEOGENE	PLIOCENE	Chinshui Shale		NN16
3.60			Kueichulin Fm	Yutengping Sandstone	NN15
5.33		Shihliufen Shale		NN13	
		Nanchuang Fm	Kuantaoshan Sandstone	NN12	
MIOCENE			Shangfuchi Sst	NN11	
		Tungkang Fm	NN10		
			NN9		
		Nankang Fm	NN8		
Kuanyinshan Sandstone			NN7		
15.97		Talu Shale	NN6		
	NN5				
	Peiliao Sandstone	NN4			
		NN3			
23.03	PALEOGENE	OLIGOCENE	Shiti Fm	NN2	
			Taliao Fm	NN1	
			Mushan Fm	NP25	
			Paleng Fm	NP24	
			Wuchishan Fm		

FIGURE 3 Chronostratigraphic correlation of sedimentary strata in north-central to southern parts of the Western Foothills of Taiwan (after Teng et al. (1991) and Chen (2016)). The studied formation is highlighted in the red box. Yellow denotes that the main lithology is comprised of sandstone, and grey indicates shale. Nannofossil zonations (NN) are derived from (Chang & Chi, 1983; Horng & Shea, 2007; Huang, 1976; Pan et al., 2015; Shea & Huang, 2003). The abbreviation Fm denotes formation.

Sandstone and the overlying Shihliufen Shale occurred near the Miocene–Pliocene transition at ca. 5.3 Ma. The first occurrence of *C. rugosus* was identified in the upper-middle Shihliufen Shale (Huang, 1976). The biozone boundary between NN12 and NN13 is defined by the boundary between the *C. tricorniculatus* and the *C. rugosus* zones (Martini, 1971), and the absolute

age for the first occurrence of *C. rugosus* is 5.12 Ma (Raffi et al., 2006). Consequently, the Shihliufen Shale–Yutengping Sandstone boundary should be slightly younger than 5.12 Ma (Figure 3).

The Taiwan orogen is recognized for its high exhumation rates. Fission-track thermochronometry reveals that exhumation rates for the entire orogenic belt ranges from 3 to 5 mm yr⁻¹ following the early onset of collision (Liu et al., 2000; Willett et al., 2003). In contrast, other studies have shown that exhumation rates were slow during early stages of orogenesis (<1 mm yr⁻¹ prior to 1–2 Ma), then rapidly accelerated to 2–4 mm yr⁻¹ after 1–2 Ma, and to 4–10 mm yr⁻¹ ca. 0.5 Ma to (Hsu et al., 2016; Kirstein et al., 2010; Lai et al., 2022; Lee et al., 2006). The initiation of brittle extension at 1.6 Ma also coincides with rapid acceleration in exhumation and sediment accumulation in the WFB (Chen et al., 2022). While uplift and erosion rates during early emergence of the Taiwan orogen may have been slower than today, high volumes of sediment were probably liberated by earthquakes and through erosion of poorly lithified sedimentary strata; these sediment were subsequently delivered to adjacent seas during periods of high precipitation (i.e. during tropical cyclones or monsoons) as in the present day (Dadson et al., 2003; Hilton et al., 2010; Kao et al., 2014; Lin et al., 2020). Furthermore, in the Pliocene, it is likely that the warmer climate produced more intense and frequent tropical cyclones and monsoons than at present (Coumou & Rahmstorf, 2012; Dashtgard et al., 2021; Kelman, 2013; Kossin, 2018; Kossin et al., 2020).

2 | METHODS

This study focuses on a 429-m-thick section that extends through most of the Kueichulin Formation (from the upper Kuantaoshan Sandstone through the majority of the Yutengping Sandstone) that outcrops along the Da'an River in central Taiwan (Figure 2b). Thickness measurements of the Kueichulin Formation were taken using a Jacob's staff and a digital inclinometer. Sedimentological descriptions include lithology, grain size, sedimentary structures, bedding contacts and accessory structures. Ichnological descriptions include trace-fossil identifications and bioturbation index assessments (BI; Reineck, 1963; Taylor & Goldring, 1993). The basal 0–62.7 m and upper 264.2–429.0 m of outcrop were logged for this paper, and the intervening 201.5 m (62.7–264.2 m) were described for sedimentology, ichnology and geochemistry of C and N by Dashtgard et al. (2020, 2021). The outcrop section was sampled for clay mineralogy, organic carbon and nitrogen content and geochemistry and magnetic susceptibility.

2.1 | Clay mineralogy

Fifty-two samples were collected for clay mineral analysis at the Institute of Oceanography at National Taiwan University, Taiwan. On average, one sample was collected every 8.2 m, but sampling frequency depended on the availability of mudstone beds. Samples were prepared according to procedures described by Biscaye (1965), Hauff et al. (1984) and Poppe et al. (2001). Samples were crushed using an agate mortar and pestle and passed through a sieve to collect grains <64 µm in diameter. The resulting powder was mixed with a 1% sodium hexametaphosphate solution to disperse clay minerals. The grain size fraction greater than 2 µm was removed through suspension settling, and clay fractions (<2 µm) were then decanted from the top of the sample solution and pipetted onto glass slides. Oriented mounts of clay minerals were prepared by allowing the sample to settle onto glass slides by gravity and air drying. The samples were then saturated in ethylene-glycol for 8 h, followed by heating to 550°C for 6 h. Samples were scanned three times using a Rigaku Miniflex II X-ray diffractometer (XRD). X-ray diffraction analyses were used to identify illite, chlorite, smectite and kaolinite. The proportions of each clay mineral were estimated using the MDI JADE® software. Illite crystallinity was also measured based on the width at half-height of the 10 Å peak (2θ at 8.8°) and calibrated to the Kübler Index (°Δ2θ); decreasing °Δ2θ values correspond to increasing illite crystallinity (Kübler & Jaboyedoff, 2000).

2.2 | Elemental and carbon isotope compositions of organic matter

A total of 272 samples were collected and analysed for organic geochemistry; this includes 118 new samples collected in 2021 and 154 collected and analysed previously (Dashtgard et al., 2021). Samples were collected every 1.6 m (on average) vertically through the stratigraphic section. All samples were analysed for δ¹³C_{org}, total organic carbon and total nitrogen at the Stable Isotope Laboratory at National Taiwan University, Taiwan. δ¹³C_{org} was measured using an elemental analyser (Flash EA, Thermo Scientific) coupled to an isotope ratio mass spectrometer (Delta V Advantage, Thermo Scientific), and total organic carbon and total nitrogen were measured using an elemental analyser (Vario Micro Cube, Elementar). δ¹³C_{org} and C/N values are compared with published values to assess the source and degree of mixing of organic carbon in the sediment (Table 1; Dashtgard et al., 2021). To semi-quantify the amount of mixing and determine the percentage of marine organic matter (and by extension the

percentage of terrestrial organic matter), a simple stable isotope mixing equation is used (Equation 1):

$$\% \text{ Marine Organic Matter} = \frac{\delta^{13}\text{C}_{\text{sample}} - \delta^{13}\text{C}_{\text{terrestrial}}}{\delta^{13}\text{C}_{\text{marine}} - \delta^{13}\text{C}_{\text{terrestrial}}} \times 100\% \quad (1)$$

δ¹³C_{marine} represents the δ¹³C value for marine organic matter (−21.8‰ ± 1.7‰; Dashtgard et al., 2021), and δ¹³C_{terrestrial} represents the average of δ¹³C values for C3 plants, soil and suspended particulate organic matter in the modern Da'an River (−25.7‰ ± 1.1‰; Dashtgard et al., 2021; Hilton et al., 2010).

2.3 | Mass-specific magnetic susceptibility

Sixty-six oriented palaeomagnetic core samples (25 mm diameter) were collected approximately every 6.4 m vertically from unweathered, mud-rich beds. The orientation of each core was measured using a mechanical device with a magnetic compass. Cores were cut into 2-cm-long specimens, and mass-specific magnetic susceptibility (χ) of the specimen was obtained by measuring its bulk magnetic susceptibility using a Bartington Instruments MS2B magnetic susceptibility meter and dividing by its weight.

3 | RESULTS

3.1 | Sedimentology and stratigraphy

The outcrop section logged along the Da'an River is divided into six stratigraphic intervals based on sedimentological and biogenic features, and palaeo-water depths are derived from previous studies (Figure 4a; Dashtgard et al., 2020, 2021; Nagel et al., 2013). The uppermost part of the Kuantaoshan Sandstone (0–62.7 m interval) comprises low-BI, wavy laminated to trough cross-stratified to hummocky cross-stratified sandstone (0–17 m), overlain by moderately to highly bioturbated silty to muddy sandstone (17–62.7 m). These strata are interpreted to represent deposition in water depths ranging from 25 to 35 m, which is above estimated storm wave base (Nagel et al., 2013). The overlying Shihliufen Shale comprises dark-grey fossiliferous mudstone (62.7–96.7 m) in which BI and trace fossils are generally not discernible due to lack of contrast between mud-filled burrows and the mudstone matrix. The Shihliufen Shale is interpreted to represent offshore mudstone deposited in water depths deeper than 35 m (Dashtgard et al., 2021; Nagel et al., 2013).

The Shihliufen Shale transitions upwards into the Yutengping Sandstone (96.7–429 m interval). The base of the Yutengping Sandstone comprises highly bioturbated sandy mudstone to muddy sandstone (96.7–135.7 m). Preservation of these biogenically reworked sediment is interpreted to reflect limited storm reworking of the sea-floor in water depths between 25 and 35 m (Dashtgard et al., 2020, 2021; Nagel et al., 2013). Within this interval, rare storm beds exist, and these are interpreted as tropical cyclone deposits (Dashtgard et al., 2020). The interval between 135.7 and 158.7 m is characterized by wavy- and lenticular-bedding, current ripple-lamination, hummocky cross-stratification and trough cross-stratification. Palaeo-water depths estimated for the transition zone are 20–25 m. The transition zone is overlain by a succession of mainly low-BI heterolithic mudstone and sandstone (158.7–429 m), and these strata are interpreted to record deposition under dominantly tidal influence and at water depths of 10–20 m. Two tropical cyclone beds are identified in the low-BI heterolithics (Dashtgard et al., 2020).

3.2 | Clay mineralogy

The dominant clay minerals in mudstone beds throughout the Kueichulin Formation are illite and chlorite with variable proportions of smectite and kaolinite; on average, illite and chlorite comprise >60% of clay minerals (Table 1). The relative abundance of illite is lowest in the Kuantaoshan Sandstone, increases to a maximum in the Shihliufen Shale, and decreases at the base of the Yutengping Sandstone through the high-BI sandy mudstone to muddy sandstone (Table 1; Figure 4b). Both kaolinite and chlorite show a sharp decrease in abundance from the Kuantaoshan Sandstone into the Shihliufen Shale, and both clay mineral proportions remain low in the Yutengping Sandstone (Table 1; Figure 4b). Smectite appears to be more variable, but generally increases in abundance upwards (Table 1; Figure 4b). Kübler Index values ($^{\circ}\Delta 2\theta$) also show a gradually decreasing trend upwards from the Kuantaoshan Sandstone to the Shihliufen Shale, indicating increasing illite crystallinity, but there is no net change in illite crystallinity through the Yutengping Sandstone (Figure 4b).

3.3 | $\delta^{13}\text{C}_{\text{org}}$ and C/N

The low-BI sandstone and high-BI muddy sandstone of the Kuantaoshan Sandstone exhibit the highest $\delta^{13}\text{C}_{\text{org}}$ values in the logged succession and have intermediate C/N values (Figures 4c and 5; Table 1). $\delta^{13}\text{C}_{\text{org}}$ decreases abruptly from the Kuantaoshan Sandstone into the lower Shihliufen Shale,

TABLE 1 Summary of clay mineralogy, $\delta^{13}\text{C}_{\text{org}}$ and C/N, % marine organic carbon (OC) and mass-specific magnetic susceptibility (χ) from the Kueichulin Formation exposed along Da'an River, Taiwan

	Smectite (%)	Kaolinite (%)	Illite (%)	Chlorite (%)	$\delta^{13}\text{C}_{\text{org}}$ (‰)	C/N	% Marine OC	χ ($10^{-7} \text{ m}^3 \text{ kg}^{-1}$)
<i>Yutengping Sandstone</i>								
Low-BI Heterolithics	22 ± 16 (16)	20 ± 6 (16)	39 ± 12 (16)	20 ± 11 (16)	-26.6 ± 0.4 (128)	8.5 ± 1.7 (128)	1.0 ± 4.2 (128)	1.3 ± 0.4 (23)
Transition	25 ± 5 (9)	19 ± 6 (9)	39 ± 7 (16)	18 ± 3 (9)	-26.3 ± 0.5 (49 ^a)	8.4 ± 2.2 (49 ^a)	3.8 ± 7.1 (49 ^a)	2.0 ± 1.2 (38)
High-BI Muddy Sandstone	23 ± 16 (9)	17 ± 6 (9)	43 ± 11 (16)	17 ± 4 (9)	-25.9 ± 0.5 (33)	8.1 ± 1.6 (33)	10.4 ± 9.5 (33)	1.1 ± 0.3 (10)
Average	22.7 ± 13.5 (34)	19.4 ± 5.8 (34)	40 ± 10.1 (34)	18.2 ± 7.7 (34)	-26.2 ± 0.7 (212)	8.5 ± 2.2 (212)	6.1 ± 10.4 (212)	1.5 ± 0.7 (71)
<i>Shihliufen Shale</i>								
Dark grey mudstone	14 ± 11 (10)	15 ± 3 (10)	49 ± 12 (16)	22 ± 3 (10)	-24.2 ± 0.5 (31)	5.3 ± 0.5 (31)	46.1 ± 10.4 (31)	2.8 ± 1.1 (10)
Average	13.9 ± 10.8 (10)	15.2 ± 3.1 (10)	48.7 ± 11.6 (10)	22.1 ± 3.5 (10)	-24.2 ± 0.5 (31)	5.3 ± 0.5 (31)	46.1 ± 10.4 (31)	2.8 ± 1.1 (10)
<i>Kuantaoshan Sandstone</i>								
High-BI muddy sandstone	12 ± 12 (7)	28 ± 12 (7)	28 ± 8 (16)	32 ± 15 (7)	-23.3 ± 0.2 (8)	6.0 ± 0.4 (8)	66.0 ± 5.4 (8)	3.4 ± 0.5 (8)
Low-BI sandstone	10 (1)	19 (1)	41 (1)	30 (1)	-23.9 ± 0.4 (2)	6.1 ± 0.3 (2)	53.6 ± 8.4 (2)	-
Average	11.6 ± 11.2 (8)	26.7 ± 11.9 (8)	29.8 ± 8.6 (8)	31.9 ± 13.5 (8)	-23.6 ± 0.3 (10)	6.1 ± 0.4 (10)	59.8 ± 6.9 (10)	3.4 ± 0.5 (8)

Note: Values are given as: mean ± standard deviation (n); n—number of samples in each measurement.
^aOutliers at 321.4 m and 322.6 m were not included in calculations.

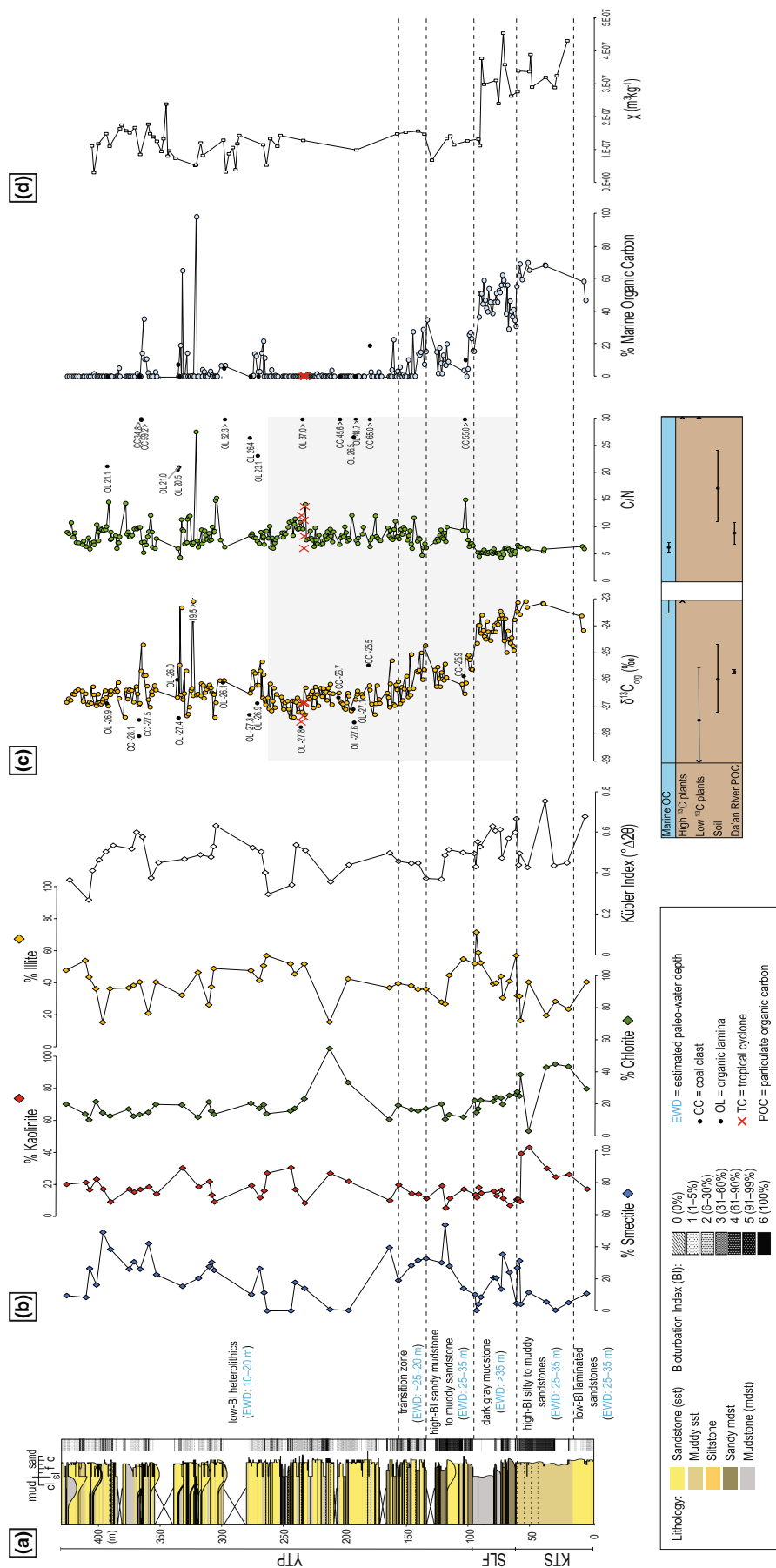


FIGURE 4 (a) Stratigraphic log of the Kueichulin Formation exposed along the Da'an River, Taiwan. Stratigraphic units include (from the base to the top), Kuantaoshan Sandstone (KTS: 0–62.7 m), Shihliufen Shale (SLF: 62.7–96.7 m) and Yutengping Sandstone (YTP: 96.7–429 m). Grain size abbreviations: cl—clay; sl—silt; f—fine-grained sand; c—coarse-grained sand. (b) Variability in clay mineral proportions (%) and illite crystallinity. Decreasing Kübler index (°Δ2θ) values correspond to increasing illite crystallinity. (c) δ¹³C_{org} and C/N values of mudstone beds sampled throughout the succession, and percentages of marine organic carbon calculated for each sample location. δ¹³C_{org} and C/N for various marine (blue) and terrestrial (brown) organic matter are shown in the table below (dots)—Means; error bars—Standard deviations; OC—Organic carbon; POC—Particulate organic carbon). Data values outside of the range shown in the graphs are indicated by the '>' symbol. (d) Mass-specific magnetic susceptibility (χ) of core samples showing a sharp decrease across the Shihliufen Shale–Yutengping Sandstone boundary. Data within the grey rectangle are derived from Dastigard et al. (2021).

and then increases up-section through the shale; C/N shows only a slight decrease in values upwards through the same interval. Overall, the Yutengping Sandstone has the lowest $\delta^{13}\text{C}_{\text{org}}$ values (with the exception of two anomalously high values at 332.6 m and 321.4 m) and the highest C/N (Figure 4c). In the Yutengping Sandstone, $\delta^{13}\text{C}_{\text{org}}$ values decrease upwards from the high-BI muddy sandstone through the transition zone and into the low-BI heterolithics. $\delta^{13}\text{C}_{\text{org}}$ values for five samples collected from three tropical cyclone beds and 14 samples collected from coal and organic lamina are $-27.1\text{‰} \pm 0.3\text{‰}$ and $-26.9\text{‰} \pm 0.8\text{‰}$ respectively. Tropical cyclone beds have C/N of 10.3 ± 3.1 and coal and organic lamina samples have C/N of 38.3 ± 15.8 . Based on the stable carbon isotope mixing model, the low-BI sandstone and high-BI muddy sandstone of the Kuantaoshan Sandstone contain the highest percentage of marine organic matter with $53.6\% \pm 8.4\%$ and $66.0\% \pm 5.4\%$ respectively (Table 1; Figure 4c). The percentage of marine organic matter dramatically decreases upsection. Dark grey mudstones from the Shihliufen Shale contains $46.1\% \pm 10.4\%$ marine organic matter, and in the Yutengping Sandstone, this decreases upwards from $10.4\% \pm 9.5\%$ in the high-BI muddy sandstone to $1.0\% \pm 4.2\%$ in the low-BI heterolithics (Table 1; Figure 4c).

3.4 | Mass-specific magnetic susceptibility

Mass-specific magnetic susceptibility (χ) decreases drastically from the Kuantaoshan Sandstone and Shihliufen

Shale to the Yutengping Sandstone, which indicates that the magnetic mineral concentrations are the lowest in the Yutengping Sandstone (Table 1; Figure 4d). Samples from the Kuantaoshan Sandstone have χ values of $3.4 \pm 0.5 \times 10^{-7} \text{ m}^3 \text{ kg}^{-1}$, and Shihliufen Shale samples have χ values of $2.8 \pm 1.1 \times 10^{-7} \text{ m}^3 \text{ kg}^{-1}$. In the Yutengping Sandstone χ values vary from $1.1 \pm 0.3 \times 10^{-7} \text{ m}^3 \text{ kg}^{-1}$ in the high-BI muddy sandstone to $2.0 \pm 1.2 \times 10^{-7} \text{ m}^3 \text{ kg}^{-1}$ in the transition zone, and to $1.3 \pm 0.4 \times 10^{-7} \text{ m}^3 \text{ kg}^{-1}$ in the low-BI heterolithics.

4 | DISCUSSION

4.1 | A change in sediment source in the early Pliocene

The combination of clay mineralogy, $\delta^{13}\text{C}_{\text{org}}$, C/N and mass-specific magnetic susceptibility data reveal a significant change in sediment source to the WFB during the early Pliocene, from one that is dominated by the Eurasian continent to one that is dominated by the Taiwan orogen. The evidence to support this hypothesis is detailed below.

Clay minerals from sediment delivered to the South China Sea by modern rivers can be divided into three end-members (Figure 6). First, clay minerals delivered by rivers in Taiwan are dominated by immature illite and chlorite produced by physical erosion in the Taiwan orogenic belt. Second, clay minerals from the Eurasian continent are rich in kaolinite, which is attributed to chemical weathering of feldspars. Third, clay minerals derived from

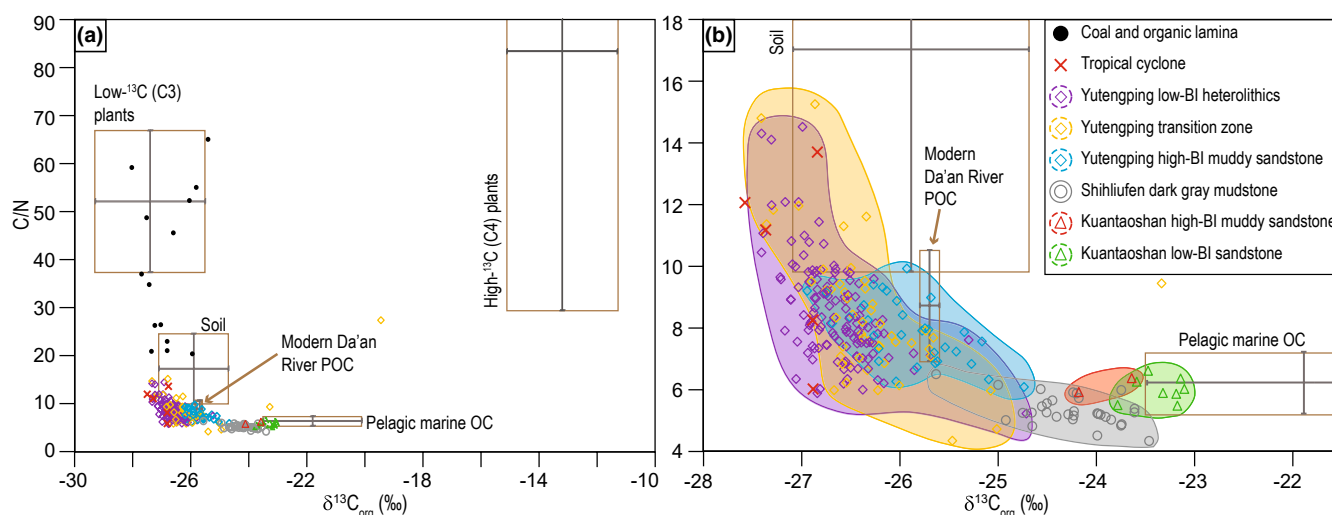


FIGURE 5 (a) Cross-plot of $\delta^{13}\text{C}_{\text{org}}$ and C/N for all samples from the Kueichulin Formation ($n = 272$). The mean and standard deviation for $\delta^{13}\text{C}_{\text{org}}$ and C/N of C3 and C4 plants, soil, modern Da'an River particulate organic carbon (POC) and pelagic marine organic carbon (OC) are shown in boxed crosses where the mean of each organic source is situated at the centre of the cross, and the standard deviation defines the length of the limbs (and size of the box). (b) An enlargement of Figure (a), showing ranges of values for each stratigraphic interval identified in this study (BI—bioturbation index).

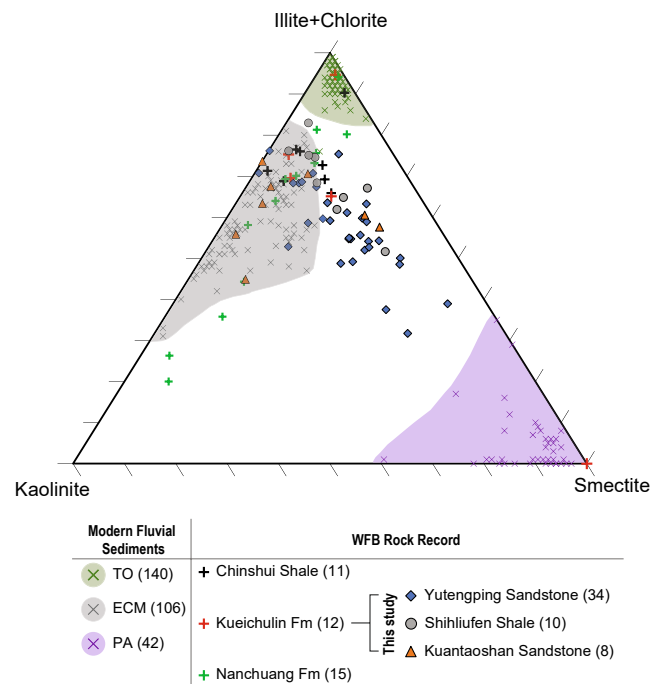


FIGURE 6 Ternary diagram of clay mineral assemblages from mudstone samples collected from the Yutengping Sandstone, Shihliufen Shale and Kuantaoshan Sandstone (this study) compared with clay mineralogy from modern fluvial sediment from the Taiwan orogen (TO; Liu, Tuo, et al., 2008), the Eurasian continental margin (ECM; Liu, Colin, Huang, Chen, et al., 2007; Liu, Colin, Huang, Le, et al., 2007) and the Philippine Archipelago (PA; Liu et al., 2009; Liu, Tuo, et al., 2008). Clay mineralogy from additional bedrock samples of the WFB (Chinshui Shale, Kueichulin Formation and Nanchuang Formation) were analysed by Huang et al. (2012) and Nagel et al. (2014). Numbers in brackets denote numbers of samples analysed.

volcanic sources have high smectite content, similar to clay minerals weathered from the Philippine Archipelago.

In the rock record, mudstones from the WFB (Nanchuang Formation to the Chinshui Shale; Figure 3) have higher proportions of kaolinite and smectite than modern fluvial clay samples from Taiwan (Figure 6; Chamley et al., 1993; Chen et al., 1992; Huang et al., 2012; Li et al., 2012; Liu, Tuo, et al., 2008). The composition of clay minerals in the Kuantaoshan Sandstone plots dominantly with Eurasian fluvial end-members, while samples from the Shihliufen Shale and Yutengping Sandstone plot closer to the Taiwan orogen and volcanic endmembers. This suggests that sediment in the WFB were derived from multiple sources (Chamley et al., 1993; Huang et al., 2012; Nagel et al., 2014), and that a major shift in the dominant sediment sources occurred at or close to the onset of deposition of the Shihliufen Shale and/or Yutengping Sandstone.

Stronger chemical weathering in hot and humid climates typically produces kaolinite, therefore, high

proportions of kaolinite in the Kuantaoshan Sandstone are attributed to long-term chemical weathering of feldspars exposed on the Eurasian continent. The abrupt decrease in kaolinite at the Kuantaoshan–Shihliufen boundary (Miocene–Pliocene transition; Figures 3 and 4b) and into the Shihliufen Shale records the rapid, relative decrease in sediment contributed from the Eurasian continent during rapid uplift and erosion of the Taiwan orogen beginning in the early Pliocene. Large contributions of clay derived from physical weathering of the Taiwan orogen diluted and overwhelmed kaolinite-rich sediment contributions from the Eurasian continent, resulting in higher relative chlorite and illite concentrations in the sediment (Figures 4b and 6; Chamley et al., 1993; Huang et al., 2012; Li et al., 2012). However, while illite increases from the Kuantaoshan Sandstone to the Shihliufen Shale, in the Yutengping Sandstone, the range of illite concentrations is similar to those in the Kuantaoshan Sandstone. Illite crystallinity also increases through the Kuantaoshan Sandstone and Shihliufen Shale, with no net change in the Yutengping Sandstone (Figure 4b). Additionally, chlorite shows a gradually decreasing trend upwards through the entire section (Figure 4b). The lack of a continuing increase in illite, illite crystallinity, and chlorite in syn-orogenic sediment, as would be expected with increasing uplift and erosion of the Taiwan orogen, is attributed to sediment recycling of the Taiwan orogenic wedge in the WFB, and this concurs with previous studies on sandstone petrography (Chen et al., 1992, 2000; Chen, Lee, et al., 2019; Nagel et al., 2014). The upwards increase in smectite may record erosion of regional volcanic sources near the Taiwan orogen.

$\delta^{13}\text{C}_{\text{org}}$ values are high and C/N values are low through the Kuantaoshan Sandstone and Shihliufen Shale, and this reflects the high proportions of marine carbon in these two members of the Kueichulin Formation. (Table 1). In contrast, $\delta^{13}\text{C}_{\text{org}}$ values are lowest and C/N values are highest in the Yutengping Sandstone, suggesting that the degree of terrestrially derived input increases upsection (i.e. marine carbon is highly diluted; Table 1; Figure 4c). In fact, the low $\delta^{13}\text{C}_{\text{org}}$ values and high C/N values in the Yutengping Sandstone (excluding two outliers) overlap with the signature of particulate organic carbon found in soil and sediment delivered by the modern-day Da'an River, suggesting that nearly the entire shallow-marine succession of the Yutengping Sandstone comprises sediment sourced overwhelmingly from the terrestrial realm (Figure 5; Dashtgard et al., 2021). The two anomalously high $\delta^{13}\text{C}_{\text{org}}$ values at 321.4 and 322.6 m (outliers) are derived from sedimentary strata that show no change in lithology or sedimentary structures to suggest a corresponding influx of marine-sourced sediment, and C/N measured at the same locations indicate a terrestrial signal. Consequently,

the two outliers are not included in statistical calculations of $\delta^{13}\text{C}_{\text{org}}$ and C/N.

The change in $\delta^{13}\text{C}_{\text{org}}$ and C/N values from the Kuantaoshan Sandstone to the Shihliufen Shale indicates that the source of organic material delivered to the palaeo-Taiwan Strait (i.e. WFB) began to change from marine to terrestrial at or close to the boundary between the two stratigraphic members. Further, the abrupt shift in carbon signatures from the Shihliufen Shale to the Yutengping Sandstone suggests that the organic source was effectively fully terrestrial in the Yutengping Sandstone. Sediment transported eastward from the Eurasian continent would have longer residence times in the ocean, resulting in increased dilution of land-derived organic material by marine organic material; this would be manifested in a more marine $\delta^{13}\text{C}_{\text{org}}$ and C/N signature (Dashtgard et al., 2021) which is recorded in the Kuantaoshan Sandstone and Shihliufen Shale (Figure 4c). The abundance of terrestrially sourced organic material in the Yutengping Sandstone indicates that land-derived organic matter was rapidly buried under the seafloor, diluting marine organic material in the sediment. Tropical cyclones are responsible for delivering a majority of terrestrially sourced organic material to the oceans in east Asia, and these weather events impacted east Asia throughout the Miocene to Recent (Coumou & Rahmstorf, 2012; Fedorov et al., 2013; Johnson, 2021; Kelman, 2013; Kossin, 2018; Kossin et al., 2020; Yan et al., 2016; Yan, Korty, et al., 2019; Yan, Wei, et al., 2019). Upon Taiwan's emergence from the Pacific Ocean in the late Miocene to early Pliocene, erosion of strata from Taiwan would have contributed significant quantities of sediment to the surrounding ocean, including the WFB, and hence, the marked increase in terrestrial (plant- and soil-derived) organic carbon observed from the Kuantaoshan Sandstone into the Shihliufen Shale records the onset of sedimentation from Taiwan, and the abrupt shift in carbon signatures from the Shihliufen Shale to the Yutengping Sandstone probably reflects the shift in the dominant sediment source from Eurasia to Taiwan.

Finally, the abrupt decrease in magnetic susceptibility observed at the top of the Shihliufen Shale upwards into the Yutengping Sandstone is attributed to a change in sediment source from the Eurasian continent to one that is dominated by the Taiwan orogen (Figure 4d). Specifically, the decrease in magnetic susceptibility in the Yutengping Sandstone marks the intensive denudation of metasedimentary rocks of the Taiwan orogen, which are depleted in magnetic minerals compared to the Eurasian continent. This resulted in magnetic minerals being diluted by the high sediment flux of non-magnetic minerals delivered from the orogen (Horng & Huh, 2011). However, the magnetic susceptibility does not record the onset of changing sediment sources near the boundary between

the Kuantaoshan Sandstone and Shihliufen Shale, and this differs from the trends seen in clay mineralogy, and $\delta^{13}\text{C}_{\text{org}}$ and C/N values.

The delayed shift in the magnetic susceptibility may reflect the initial erosion of older (passive margin) seafloor strata that was uplifted during the early stages of Taiwan orogenesis and prior to exposure and erosion of the metasedimentary core. Pre-Taiwan orogenesis, the seafloor sediment that comprise the passive-margin strata was largely derived from Eurasia and is enriched in magnetic minerals (Horng & Huh, 2011). As proto-Taiwan began to uplift, the passive margin strata that formed the island would have been exposed and vegetated, and subsequently physically eroded. The sediment eroded from proto-Taiwan was deposited in the WFB, resulting in the shift in clay mineralogy and organic carbon signatures from the Kuantaoshan Sandstone through the Shihliufen Shale. In contrast, magnetic susceptibility remained high (recording a dominant Eurasian signature) until the deposition of the Yutengping Sandstone, when low-magnetic-susceptibility sediment derived from the metasedimentary core of Taiwan was mixed with, and diluted, sediment derived from erosion of passive-margin strata of Eurasia.

4.2 | Implications for the evolution of the Taiwan Western Foreland Basin

Variations in clay mineralogy, carbon and nitrogen geochemistry, and magnetic susceptibility through the Kueichulin Formation allow us to decipher the tectonic evolution of the Taiwan orogen; consequently, the Kueichulin Formation can be used to resolve sediment provenance from adjacent continental masses to the WFB. Our results show that soon after Taiwan emerged from the Pacific Ocean, it rapidly became the dominant sediment source to the WFB and overwhelmed contributions from Eurasia (Figure 7). The abrupt shift in sediment sources from Eurasia to Taiwan began with deposition of the Shihliufen Shale, near the Miocene–Pliocene transition, and this coincides with the early stages of collision between the Eurasian Plate and the Luzon Arc on the Philippine Sea Plate. By the time the Yutengping Sandstone was being deposited just after 5.12 Ma, sediment was overwhelmingly being derived from the Taiwan orogen. This indicates that the Taiwan orogen became the dominant source to the WFB approximately two million years earlier than previously hypothesized (e.g. Chamley et al., 1993; Chang & Chi, 1983; Chen et al., 1992, 2000; Chou, 1972; Covey, 1986; Horng et al., 2012; Nagel et al., 2013, 2014, 2018; Teng, 1990).

From the early Pliocene to the present day, the palaeogeography of the WFB does not appear to have changed

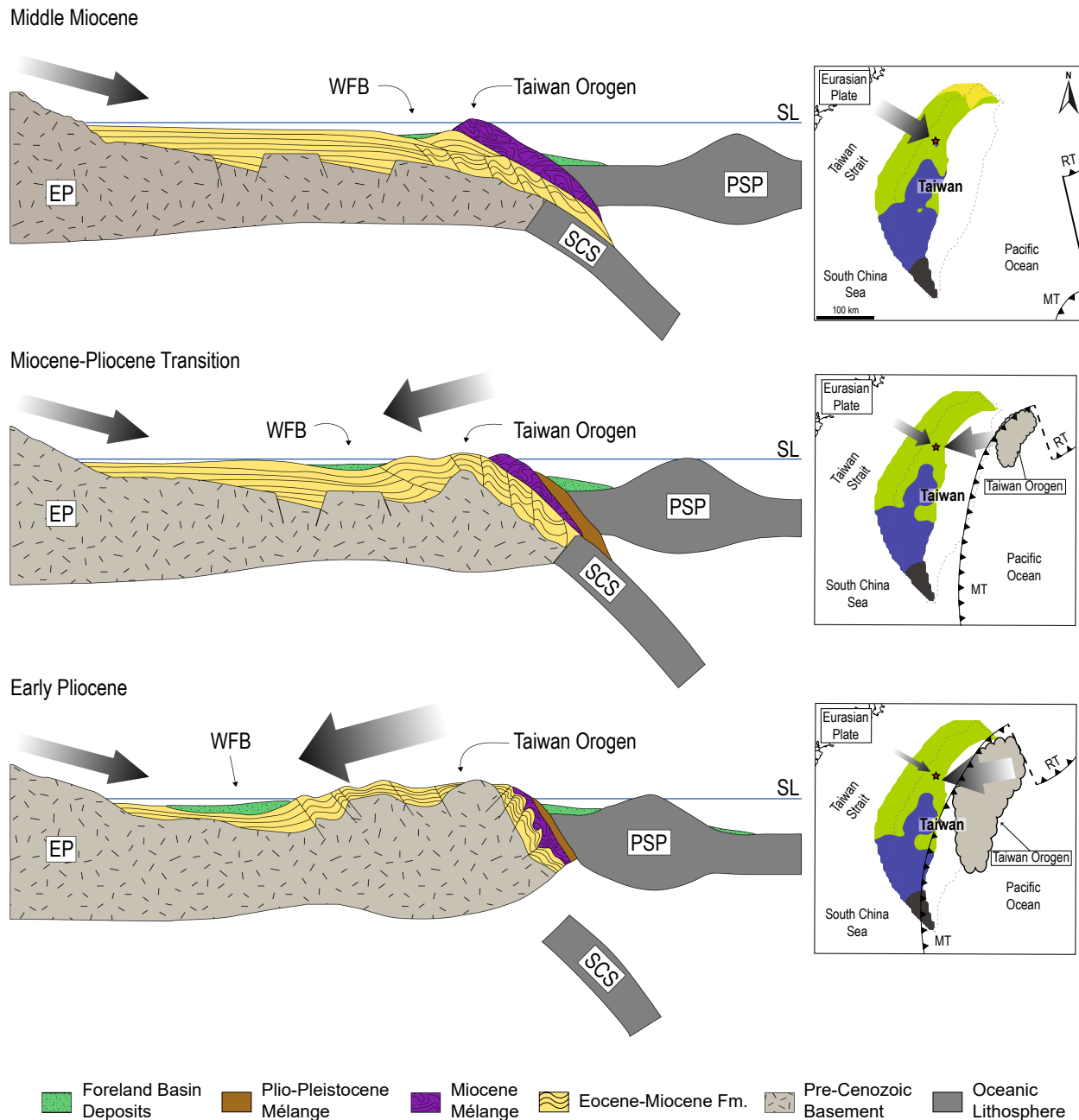


FIGURE 7 Conceptual model of sediment deposition to the WFB from the middle Miocene to the early Pliocene (modified after Chen, Yeh, & Syu, 2019; Lin et al., 2003; Nagel et al., 2013; Teng, 1990). The size of the arrows indicates relative proportions of sediment contribution from the Eurasian Plate (EP) and the emerging Taiwan orogen (SCS—South China Sea Plate; PSP—Philippine Sea Plate; RT—Ryuku Trench; MT—Manila Trench; SL—sea level). Refer to Figure 1 for the palaeo-water depth legend.

substantially (Nagel et al., 2013). The uplift of Taiwan created the Taiwan Strait, and this confined and accelerated ocean currents and tidal currents between Eurasia and Taiwan. These currents remobilize seafloor sediments and transport them towards the South and East China Seas (Milliman et al., 2007; Nagel et al., 2018), and have probably done so since the inception of the Taiwan orogen. Growth of the Taiwan orogen also propagated south-southwest since its emergence (Suppe, 1981), resulting in uplift and rapid erosion of poorly lithified

sediment in southern Taiwan (Dadson et al., 2003, 2004). Consequently, sediment loads to the study area should have been higher in the Pliocene at a time when Taiwan was situated further to the north-northeast, although the exact position of the Taiwan orogen relative to the study area remains uncertain. In the present-day, sediment is liberated from the Taiwan orogen by earthquakes and landslides. These sediment are then transported to the Taiwan Strait through fluvial drainage systems, largely during massive precipitation and runoff associated with

tropical cyclones (Chen et al., 2018; Dadson et al., 2004; Dashtgard et al., 2021; Kao & Milliman, 2008; Milliman et al., 2017; Milliman & Kao, 2005; Steer et al., 2020; Vaucher et al., 2021; Yang et al., 2022). Because the morphology, tectonic setting and evolution of Taiwan has remained largely unchanged since the early Pliocene (Lin et al., 2003; Lin & Watts, 2002; Nagel et al., 2013, 2014, 2018), the processes that eroded and delivered sediment from the Taiwan orogen to the palaeo-Taiwan Strait are likely analogous to the present-day.

5 | CONCLUSION

Here, we evaluated the timing of denudation of Taiwan by analysing various proxies preserved in the stratigraphic record to resolve and distinguish sediment sources to the Western Foreland Basin. The WFB was traditionally considered to receive sediment largely from the Eurasian continent until the late Pliocene. However, clay mineralogy, $\delta^{13}\text{C}_{\text{org}}$ and C/N values of organic material, and mass-specific magnetic susceptibility of the Kueichulin Formation reveal a major shift in sediment sources occurred approximately two million years earlier than previously proposed.

Variations in major clay minerals record the onset of changing sediment sources in the late Miocene-early Pliocene. Specifically, the decrease in kaolinite and corresponding relative increase in illite and chlorite at the Kuantaoshan Sandstone-Shihliufen Shale boundary point to a change in sediment source from the Eurasian continent (kaolinite source) to the Taiwan orogen (illite and chlorite source) by 5.3 Ma. $\delta^{13}\text{C}_{\text{org}}$ and C/N values, and mass-magnetic susceptibility reflect the volumes and transport distances of sediment delivered to the WFB. At the Shihliufen Shale-Yutengping Sandstone boundary near 5.12 Ma, there was a marked increase in terrestrial organic material and dilution of magnetic mineral concentrations in sediment delivered to the WFB. This probably reflects much higher sediment erosion rates and decreased transport distances to the WFB from the Taiwan orogen. Our findings demonstrate that the sedimentary archive of the Kueichulin Formation provides a record of the onset of rapid uplift and erosion of the Taiwan orogen, and shows that a rapid shift in sediment sources to the WFB occurred during the Miocene–Pliocene transition, with the Taiwan orogen becoming the dominant sediment source by the early Pliocene.

ACKNOWLEDGEMENTS

This research was financially supported by a Natural Sciences and Engineering Research Council of Canada Discovery Grant to S. Dashtgard (RGPIN-2019-04528),

and a Ministry of Science and Technology (Taiwan) Grant to L. Löwemark (MOST 107-2116-M-002-011). Funding was also provided by the ‘The Featured Areas Research Center Program’ within the framework of the Higher Education Sprout Project by the Ministry of Education in Taiwan. The authors thank Romy Ari Setiaji and Yu-Hsuan Liou for their assistance in the field. We are also grateful for the constructive feedback from Prof. Rebecca Dorsey and the anonymous reviewer, which helped to improve this manuscript.

CONFLICT OF INTEREST


The authors declare no conflict of interest.


DATA AVAILABILITY STATEMENT

The data that support the findings of this study are available from the corresponding author upon reasonable request.

ORCID

Amy I. Hsieh  <https://orcid.org/0000-0002-1474-1120>

Shahin E. Dashtgard  <https://orcid.org/0000-0002-7763-2300>

Chorng-Shern Horng  <https://orcid.org/0000-0003-2023-4763>

Chih-Chieh Su  <https://orcid.org/0000-0002-7624-1607>

Andrew T. Lin  <https://orcid.org/0000-0001-9284-3678>

Romain Vaucher  <https://orcid.org/0000-0003-3051-4128>

Ludvig Löwemark  <https://orcid.org/0000-0002-3337-2367>

<https://orcid.org/0000-0003-3051-4128>

<https://orcid.org/0000-0002-3337-2367>

<https://orcid.org/0000-0002-3337-2367>

<https://orcid.org/0000-0002-3337-2367>

REFERENCES

- Biscaye, P. E. (1965). Mineralogy and sedimentation of recent deep-sea clay in the Atlantic Ocean and adjacent seas and oceans. *Geological Society of America Bulletin*, 76, 803–831. [https://doi.org/10.1130/0016-7606\(1965\)76\[803:MASORD\]2.0.CO;2](https://doi.org/10.1130/0016-7606(1965)76[803:MASORD]2.0.CO;2)
- Castelltort, S., Nagel, S., Mouthereau, F., Lin, A. T.-S., Wetzell, A., Kaus, B., Willett, S., Chiang, S.-P., & Chiu, W.-Y. (2011). Sedimentology of early Pliocene sandstones in the southwestern Taiwan foreland: Implications for basin physiography in the early stages of collision. *Journal of Asian Earth Sciences*, 40, 52–71. <https://doi.org/10.1016/j.jseaes.2010.09.005>
- Chamley, H., Angelier, J., & Teng, L. S. (1993). Tectonic and environmental control of the clay mineral sedimentation in the late Cenozoic orogen of Taiwan. *Geodinamica Acta*, 6, 135–147. <https://doi.org/10.1080/09853111.1993.11105243>
- Chang, S. S. L. (1971). Regional stratigraphy and petroleum possibilities of Miocene formations in northwestern Taiwan, China. *American Association of Petroleum Geologists Bulletin*, 55, 1838–1865. <https://doi.org/10.1306/819A3DAE-16C5-11D7-864500102C1865D>
- Chang, S. S. L., & Chi, W. R. (1983). Neogene nannoplankton biostratigraphy in Taiwan and the tectonic implications. *Petroleum Geology of Taiwan*, 19, 93–147.

- Chen, C.-H., Lee, C.-Y., Lin, J.-W., & Chu, M.-F. (2019). Provenance of sediments in western Foothills and Hsuehshan Range (Taiwan): A new view based on the EMP monazite versus LA-ICPMS zircon geochronology of detrital grains. *Earth-Science Reviews*, *190*, 224–246. <https://doi.org/10.1016/j.earscirev.2018.12.015>
- Chen, C.-T., Lo, C.-H., Wang, P.-L., & Lin, L.-H. (2022). Extensional mountain building along convergent plate boundary: Insights from the active Taiwan mountain belt. *Geology*, *50*, 1245–1249. <https://doi.org/10.1130/G50311.1>
- Chen, C.-W., Oguchi, T., Hayakawa, Y. S., Saito, H., Chen, H., Lin, G.-W., Wei, L.-W., & Chao, Y.-C. (2018). Sediment yield during typhoon events in relation to landslides, rainfall, and catchment areas in Taiwan. *Geomorphology*, *303*, 540–548. <https://doi.org/10.1016/j.geomorph.2017.11.007>
- Chen, J., Ma, J., Xu, K., Liu, Y., Cao, W., Wei, T., Zhao, B., & Chen, Z. (2017). Provenance discrimination of the clay sediment in the western Taiwan Strait and its implication for coastal current variability during the late-Holocene. *The Holocene*, *27*, 110–121. <https://doi.org/10.1177/0959683616652706>
- Chen, W. S. (2016). *An introduction to the geology of Taiwan*. Geological Society of Taiwan.
- Chen, W. S., Erh, C. H., Chen, M. M., Yang, C. C., Chang, I. S., Liu, T. K., Horng, C. S., Shea, K. S., Yeh, M. G., Chang, W. J., Te, K. C., Lin, C. C., & Huang, N. W. (2000). The evolution of foreland basins in the western Taiwan: Evidence from the Pliocene sequences. *Bulletin of the Central Geological Survey*, *13*, 137–156.
- Chen, W.-S., Yeh, J.-J., & Syu, S.-J. (2019). Late Cenozoic exhumation and erosion of the Taiwan orogenic belt: New insights from petrographic analysis of foreland basin sediments and thermochronological dating on the metamorphic orogenic wedge. *Tectonophysics*, *750*, 56–69. <https://doi.org/10.1016/j.tecto.2018.09.003>
- Chen, Z. H., Chen, W. S., Wang, Y., & Chen, M. M. (1992). Petrographical study of foreland sandstones and its relation to unroofing history of the fold-thrust belt in central Taiwan. *Ti-Chih*, *12*, 147–165.
- Chmura, G. L., & Aharon, P. (1995). Stable carbon isotope signatures of sedimentary carbon in coastal wetlands as indicators of salinity regime. *Journal of Coastal Research*, *11*, 124–135.
- Chou, J. T. (1972). A sedimentologic and paleogeographic study of the upper Cenozoic clastic sequences in the Chiayi region, western Taiwan. *Petroleum Geology of Taiwan*, *10*, 141–158.
- Chou, Y.-W., & Yu, H.-S. (2002). Structural expressions of flexural extension in the arc-continent collisional foredeep of western Taiwan. *Special Paper of the Geological Society of America*, *358*, 1–12. <https://doi.org/10.1130/0-8137-2358-2.1>
- Coumou, D., & Rahmstorf, S. (2012). A decade of weather extremes. *Nature Climate Change*, *2*, 491–496. <https://doi.org/10.1038/nclimate1452>
- Covey, M. (1986). The evolution of foreland basins to steady state: evidence from the Western Taiwan Foreland Basin. In *Foreland Basins* (pp. 77–90). Blackwell Publishing Ltd. <https://doi.org/10.1002/9781444303810.ch4>
- Czarnecki, J. M., Dashtgard, S. E., Pospelova, V., Mathewes, R. W., & MacEachern, J. A. (2014). Palynology and geochemistry of channel-margin sediments across the tidal-fluvial transition, lower Fraser River, Canada: Implications for the rock record. *Marine and Petroleum Geology*, *51*, 152–166. <https://doi.org/10.1016/j.marpetgeo.2013.12.008>
- Dadson, S. J., Hovius, N., Chen, H., Dade, W. B., Hsieh, M.-L., Willett, S. D., Hu, J.-C., Horng, M.-J., Chen, M.-C., Stark, C. P., Lague, D., & Lin, J.-C. (2003). Links between erosion, runoff variability and seismicity in the Taiwan orogen. *Nature*, *426*, 648–651. <https://doi.org/10.1038/nature02150>
- Dadson, S. J., Hovius, N., Chen, H., Dade, W. B., Lin, J.-C., Hsu, M.-L., Lin, C.-W., Horng, M.-J., Chen, T.-C., Milliman, J., & Stark, C. P. (2004). Earthquake-triggered increase in sediment delivery from an active mountain belt. *Geology*, *32*, 733. <https://doi.org/10.1130/G20639.1>
- Dashtgard, S. E., Löwemark, L., Vaucher, R., Pan, Y.-Y., Pilarczyk, J. E., & Castellort, S. (2020). Tropical cyclone deposits in the Pliocene Taiwan Strait: Processes, examples, and conceptual model. *Sedimentary Geology*, *405*, 105687. <https://doi.org/10.1016/j.sedgeo.2020.105687>
- Dashtgard, S. E., Löwemark, L., Wang, P.-L., Setiaji, R. A., & Vaucher, R. (2021). Geochemical evidence of tropical cyclone controls on shallow-marine sedimentation (Pliocene, Taiwan). *Geology*, *49*, 566–570. <https://doi.org/10.1130/G48586.1>
- DeCelles, P. G., & Giles, K. A. (1996). Foreland basin systems. *Basin Research*, *8*, 105–123. <https://doi.org/10.1046/j.1365-2117.1996.01491.x>
- Fedorov, A. V., Brierley, C. M., Lawrence, K. T., Liu, Z., Dekens, P. S., & Ravelo, A. C. (2013). Patterns and mechanisms of early Pliocene warmth. *Nature*, *496*, 43–49. <https://doi.org/10.1038/nature12003>
- Flemings, P. B., & Jordan, T. E. (1989). A synthetic stratigraphic model of foreland basin development. *Journal of Geophysical Research*, *94*, 3851–3866. <https://doi.org/10.1029/JB094iB04p03851>
- Hatfield, R. (2014). Particle size-specific magnetic measurements as a tool for enhancing our understanding of the bulk magnetic properties of sediments. *Minerals*, *4*, 758–787. <https://doi.org/10.3390/min4040758>
- Hauff, P. L., Starkey, H. C., Blackmon, P. D., & Pevear, D. R. (1984). *Sample preparation procedures for the analysis of clay minerals by X-ray diffraction*. Open-File Report, US Geological Survey.
- Hilton, R. G., Galy, A., Hovius, N., Horng, M.-J., & Chen, H. (2010). The isotopic composition of particulate organic carbon in mountain rivers of Taiwan. *Geochimica et Cosmochimica Acta*, *74*, 3164–3181. <https://doi.org/10.1016/j.gca.2010.03.004>
- Horng, C.-S., & Huh, C.-A. (2011). Magnetic properties as tracers for source-to-sink dispersal of sediments: A case study in the Taiwan Strait. *Earth and Planetary Science Letters*, *309*, 141–152. <https://doi.org/10.1016/j.epsl.2011.07.002>
- Horng, C.-S., Huh, C.-A., Chen, K.-H., Lin, C.-H., Shea, K.-S., & Hsiung, K.-H. (2012). Pyrrhotite as a tracer for denudation of the Taiwan orogen. *Geochemistry, Geophysics, Geosystems*, *13*, Q08Z47. <https://doi.org/10.1029/2012GC004195>
- Horng, C. S., & Shea, K. S. (2007). The Quaternary magnetobiostratigraphy of Taiwan and Penglai orogenic events. *Special Publication of the Central Geological Survey*, *18*, 51–83.
- Hsu, W.-H., Byrne, T. B., Ouimet, W., Lee, Y.-H., Chen, Y.-G., van Soest, M., & Hodges, K. (2016). Pleistocene onset of rapid, punctuated exhumation in the eastern central range of the Taiwan orogenic belt. *Geology*, *44*, 719–722. <https://doi.org/10.1130/G37914.1>
- Huang, A. H., Lin, A. T., Jiang, W. T., & Wu, R. Z. (2012). Clay mineralogy of the Miocene–Pleistocene sedimentary rocks, NW Taiwan. *Western Pacific Earth Sciences*, *12*, 65–84.

- Huang, T.-C. (1976). Neogene calcareous nannoplankton biostratigraphy viewed from the Chuhuangkeng section, northwestern Taiwan. *Proceedings of the Geological Society of China*, 19, 7–24.
- Johnson, M. E. (2021). Geological oceanography of the Pliocene Warm Period: A review with predictions on the future of global warming. *Journal of Marine Science and Engineering*, 9, 1210. <https://doi.org/10.3390/jmse9111210>
- Kao, S.-J., Hilton, R. G., Selvaraj, K., Dai, M., Zehetner, F., Huang, J.-C., Hsu, S.-C., Sparkes, R., Liu, J. T., Lee, T.-Y., Yang, J.-Y. T., Galy, A., Xu, X., & Hovius, N. (2014). Preservation of terrestrial organic carbon in marine sediments offshore Taiwan: mountain building and atmospheric carbon dioxide sequestration. *Earth Surface Dynamics*, 2, 127–139. <https://doi.org/10.5194/esurf-2-127-2014>
- Kao, S. J., & Liu, K. K. (2000). Stable carbon and nitrogen isotope systematics in a human-disturbed watershed (Lanyang-Hsi) in Taiwan and the estimation of biogenic particulate organic carbon and nitrogen fluxes. *Global Biogeochemical Cycles*, 14, 189–198. <https://doi.org/10.1029/1999GB900079>
- Kao, S. J., & Milliman, J. D. (2008). Water and sediment discharge from small mountainous rivers, Taiwan: the roles of lithology, episodic events, and human activities. *The Journal of Geology*, 116, 431–448. <https://doi.org/10.1086/590921>
- Kelman, I. (2013). Saffir-Simpson Hurricane Intensity Scale. In P. T. Bobrowsky (Ed.), *Encyclopedia of Natural Hazards* (pp. 882–883). Springer. https://doi.org/10.1007/978-1-4020-4399-4_306
- Kirstein, L. A., Fellin, M. G., Willett, S. D., Carter, A., Chen, Y.-G., Garver, J. I., & Lee, D. C. (2010). Pliocene onset of rapid exhumation in Taiwan during arc-continent collision: New insights from detrital thermochronometry. *Basin Research*, 22, 270–285. <https://doi.org/10.1111/j.1365-2117.2009.00426.x>
- Kodama, K. P., & Hinnov, L. A. (2015). *Rock Magnetic Cyclostratigraphy* (1st ed.). John Wiley & Sons.
- Kossin, J. P. (2018). A global slowdown of tropical-cyclone translation speed. *Nature*, 558, 104–107. <https://doi.org/10.1038/s41586-018-0158-3>
- Kossin, J. P., Knapp, K. R., Olander, T. L., & Velden, C. S. (2020). Global increase in major tropical cyclone exceedance probability over the past four decades. *Proceedings of the National Academy of Sciences*, 117, 11975–11980. <https://doi.org/10.1073/pnas.1920849117>
- Kübler, B., & Jaboyedoff, M. (2000). Illite crystallinity. *Comptes Rendus de l'Académie des Sciences—Series IIA—Earth and Planetary Science*, 331, 75–89. [https://doi.org/10.1016/S1251-8050\(00\)01395-1](https://doi.org/10.1016/S1251-8050(00)01395-1)
- Lai, L. S.-H., Dorsey, R. J., Horng, C.-S., Chi, W.-R., Shea, K.-S., & Yen, J.-Y. (2022). Extremely rapid up-and-down motions of sland arc crust during arc-continent collision. *Communications Earth & Environment*, 3, 100. <https://doi.org/10.1038/s43247-022-00429-2>
- Lee, Y.-H., Chen, C.-C., Liu, T.-K., Ho, H.-C., Lu, H.-Y., & Lo, W. (2006). Mountain building mechanisms in the Southern Central Range of the Taiwan Orogenic Belt—From accretionary wedge deformation to arc-continent collision. *Earth and Planetary Science Letters*, 252, 413–422. <https://doi.org/10.1016/j.epsl.2006.09.047>
- Li, C., Shi, X., Kao, S., Chen, M., Liu, Y., Fang, X., Lü, H., Zou, J., Liu, S., & Qiao, S. (2012). Clay mineral composition and their sources for the fluvial sediments of Taiwanese rivers. *Chinese Science Bulletin*, 57, 673–681. <https://doi.org/10.1007/s11434-011-4824-1>
- Lin, A. T., Wang, S.-M., Hung, J.-H., Wu, M.-S., & Liu, C.-S. (2007). Lithostratigraphy of the Taiwan Chelungpu-Fault Drilling Project-A borehole and its neighboring region, Central Taiwan. *Terrestrial, Atmospheric and Oceanic Sciences*, 18, 223. [https://doi.org/10.3319/TAO.2007.18.2.223\(TCDP\)](https://doi.org/10.3319/TAO.2007.18.2.223(TCDP))
- Lin, A. T., & Watts, A. B. (2002). Origin of the West Taiwan basin by orogenic loading and flexure of a rifted continental margin. *Journal of Geophysical Research: Solid Earth*, 107, ETG 2-1–ETG 2-19. <https://doi.org/10.1029/2001JB000669>
- Lin, A. T., Watts, A. B., & Hesselbo, S. P. (2003). Cenozoic stratigraphy and subsidence history of the South China Sea margin in the Taiwan region: Cenozoic stratigraphy of Taiwan. *Basin Research*, 15, 453–478. <https://doi.org/10.1046/j.1365-2117.2003.00215.x>
- Lin, B., Liu, Z., Eglinton, T. I., Kandasamy, S., Blattmann, T. M., Haghypour, N., Huang, K.-F., & You, C.-F. (2020). Island-wide variation in provenance of riverine sedimentary organic carbon: A case study from Taiwan. *Earth and Planetary Science Letters*, 539, 116238. <https://doi.org/10.1016/j.epsl.2020.116238>
- Lin, C.-W., & Chen, W.-S. (2016). *Geologic map of Taiwan*. Geological Society of Taiwan.
- Liu, J. P., Liu, C. S., Xu, K. H., Milliman, J. D., Chiu, J. K., Kao, S. J., & Lin, S. W. (2008). Flux and fate of small mountainous rivers derived sediments into the Taiwan Strait. *Marine Geology*, 256, 65–76. <https://doi.org/10.1016/j.margeo.2008.09.007>
- Liu, T.-K., Chen, Y.-G., Chen, W.-S., & Jiang, S.-H. (2000). Rates of cooling and denudation of the Early Penglai Orogeny, Taiwan, as assessed by fission-track constraints. *Tectonophysics*, 320, 69–82. [https://doi.org/10.1016/S0040-1951\(00\)00028-7](https://doi.org/10.1016/S0040-1951(00)00028-7)
- Liu, Z., Colin, C., Huang, W., Chen, Z., Trentesaux, A., & Chen, J. (2007). Clay minerals in surface sediments of the Pearl River drainage basin and their contribution to the South China Sea. *Chinese Science Bulletin*, 52, 1101–1111. <https://doi.org/10.1007/s11434-007-0161-9>
- Liu, Z., Colin, C., Huang, W., Le, K. P., Tong, S., Chen, Z., & Trentesaux, A. (2007). Climatic and tectonic controls on weathering in south China and Indochina Peninsula: Clay mineralogical and geochemical investigations from the Pearl, Red, and Mekong drainage basins. *Geochemistry, Geophysics, Geosystems*, 8, Q05005. <https://doi.org/10.1029/2006GC001490>
- Liu, Z., Tuo, S., Colin, C., Liu, J. T., Huang, C.-Y., Selvaraj, K., Chen, C.-T. A., Zhao, Y., Siringan, F. P., Boulay, S., & Chen, Z. (2008). Detrital fine-grained sediment contribution from Taiwan to the northern South China Sea and its relation to regional ocean circulation. *Marine Geology*, 255, 149–155. <https://doi.org/10.1016/j.margeo.2008.08.003>
- Liu, Z., Zhao, Y., Colin, C., Siringan, F. P., & Wu, Q. (2009). Chemical weathering in Luzon, Philippines from clay mineralogy and major-element geochemistry of river sediments. *Applied Geochemistry*, 24, 2195–2205. <https://doi.org/10.1016/j.apgeochem.2009.09.025>
- Martini, E. (1971). Standard Tertiary and Quaternary Calcareous Nannoplankton Zonation. In A. Farinacci (Ed.), *Proceedings of the Second International Conference on Planktonic Microfossils* (pp. 739–785). Rome.
- Martiny, A. C., Pham, C. T. A., Primeau, F. W., Vrugt, J. A., Moore, J. K., Levin, S. A., & Lomas, M. W. (2013). Strong latitudinal patterns in the elemental ratios of marine plankton and organic matter. *Nature Geoscience*, 6, 279–283. <https://doi.org/10.1038/ngeo1757>

- Milliman, J. D., & Kao, S. (2005). Hyperpycnal Discharge of Fluvial Sediment to the Ocean: Impact of Super-Typhoon Herb (1996) on Taiwanese Rivers. *The Journal of Geology*, *113*, 503–516. <https://doi.org/10.1086/431906>
- Milliman, J. D., Lee, T. Y., Huang, J. C., & Kao, S. J. (2017). Impact of catastrophic events on small mountainous rivers: Temporal and spatial variations in suspended- and dissolved-solid fluxes along the Choshui River, central western Taiwan, during typhoon Mindulle, July 2–6, 2004. *Geochimica et Cosmochimica Acta*, *205*, 272–294. <https://doi.org/10.1016/j.gca.2017.02.015>
- Milliman, J. D., Lin, S. W., Kao, S. J., Liu, J. P., Liu, C. S., Chiu, J. K., & Lin, Y. C. (2007). Short-term changes in seafloor character due to flood-derived hyperpycnal discharge: Typhoon Mindulle, Taiwan, July 2004. *Geology*, *35*, 779. <https://doi.org/10.1130/G23760A.1>
- MOEA. (2019). *Geology of Taiwan*. Central Geological Survey. <https://www.moeacgs.gov.tw/eng>
- Nagel, S., Castellort, S., Garzanti, E., Lin, A. T., Willett, S. D., Mouthereau, F., Limonta, M., & Adatte, T. (2014). Provenance evolution during arc-continent collision: sedimentary petrography of Miocene to Pleistocene sediments in the Western Foreland Basin of Taiwan. *Journal of Sedimentary Research*, *84*, 513–528. <https://doi.org/10.2110/jsr.2014.44>
- Nagel, S., Castellort, S., Wetzel, A., Willett, S. D., Mouthereau, F., & Lin, A. T. (2013). Sedimentology and foreland basin paleogeography during Taiwan arc continent collision. *Journal of Asian Earth Sciences*, *62*, 180–204. <https://doi.org/10.1016/j.jseaes.2012.09.001>
- Nagel, S., Granjeon, D., Willett, S., Lin, A. T.-S., & Castellort, S. (2018). Stratigraphic modeling of the Western Taiwan foreland basin: Sediment flux from a growing mountain range and tectonic implications. *Marine and Petroleum Geology*, *96*, 331–347. <https://doi.org/10.1016/j.marpetgeo.2018.05.034>
- Pan, T.-Y., Lin, A. T.-S., & Chi, W.-R. (2015). Paleoenvironments of the evolving Pliocene to early Pleistocene foreland basin in northwestern Taiwan: An example from the Dahan River section: Paleoenvironments of NW Taiwan foreland. *Island Arc*, *24*, 317–341. <https://doi.org/10.1111/iar.12113>
- Peterson, B. J., & Fry, B. (1987). Stable isotopes in ecosystem studies. *Annual Review of Ecology and Systematics*, *18*, 293–320. <https://doi.org/10.1146/annurev.es.18.110187.001453>
- Poppe, L.J., Paskevich, V.F., Hathaway, J.C., and Blackwood, D.S. 2001. *A laboratory manual for X-ray powder diffraction*. Report. <https://doi.org/10.3133/ofr0141>.
- Raffi, I., Backman, J., Fornaciari, E., Pälke, H., Rio, D., Lourens, L., & Hilgen, F. (2006). A review of calcareous nannofossil astrochronology encompassing the past 25 million years. *Quaternary Science Reviews*, *25*, 3113–3137. <https://doi.org/10.1016/j.quascirev.2006.07.007>
- Reineck, H. E. (1963). Sedimentgefüge im Bereich der südlichen Nordsee. *Abhandlungen der Senckenbergischen Gesellschaft für Naturforschung*, *505*, 1–138.
- Shaw, C.-L. (1996). Stratigraphic correlation and isopach maps of the Western Taiwan Basin. *Terrestrial, Atmospheric, and Oceanic Sciences*, *7*, 333–360. [https://doi.org/10.3319/TAO.1996.7.3.333\(T\)](https://doi.org/10.3319/TAO.1996.7.3.333(T))
- Shea, K.-S., & Huang, T. (2003). Tertiary stratigraphy in Taiwan. *The Taiwan Mining Industry*, *55*, 17–32.
- Simoes, M., & Avouac, J. P. (2006). Investigating the kinematics of mountain building in Taiwan from the spatiotemporal evolution of the foreland basin and western foothills. *Journal of Geophysical Research: Solid Earth*, *111*, B10401. <https://doi.org/10.1029/2005JB004209>
- Steer, P., Jeandet, L., Cubas, N., Marc, O., Meunier, P., Simoes, M., Cattin, R., Shyu, J. B. H., Mouyen, M., Liang, W.-T., Theunissen, T., Chiang, S.-H., & Hovius, N. (2020). Earthquake statistics changed by typhoon-driven erosion. *Scientific Reports*, *10*, 10899. <https://doi.org/10.1038/s41598-020-67865-y>
- Suppe, J. (1981). Mechanics of mountain building and metamorphism in Taiwan. *Memoir of the Geological Society of China*, *4*, 67–89.
- Taylor, A. M., & Goldring, R. (1993). Description and analysis of bioturbation and ichnofabric. *Journal of the Geological Society*, *150*, 141–148. <https://doi.org/10.1144/gsjgs.150.1.0141>
- Teng, L. S. (1990). Geotectonic evolution of late Cenozoic arc-continent collision in Taiwan. *Tectonophysics*, *183*, 57–76. [https://doi.org/10.1016/0040-1951\(90\)90188-E](https://doi.org/10.1016/0040-1951(90)90188-E)
- Teng, L. S., Wang, Y., Tang, C.-H., Huang, C.-Y., Huang, T.-C., Yu, M.-S., & Ke, A. (1991). Tectonic aspects of the Paleogene depositional basin of northern Taiwan. *Proceedings of the Geology Society of China*, *34*, 313–336.
- Thompson, R., & Oldfield, F. (1986). Magnetic properties of natural materials. In R. Thompson & F. Oldfield (Eds.), *Environmental magnetism* (pp. 21–38). Springer. https://doi.org/10.1007/978-94-011-8036-8_4
- Vaucher, R., Dashtgard, S. E., Horng, C.-S., Zeeden, C., Dillinger, A., Pan, Y.-Y., Setiaji, R. A., Chi, W.-R., & Löwemark, L. (2021). Insolation-paced sea level and sediment flux during the early Pleistocene in Southeast Asia. *Scientific Reports*, *11*, 16707. <https://doi.org/10.1038/s41598-021-96372-x>
- Willett, S. D., Fisher, D., Fuller, C., En-Chao, Y., & Chia-Yu, L. (2003). Erosion rates and orogenic-wedge kinematics in Taiwan inferred from fission-track thermochronometry. *Geology*, *31*, 945. <https://doi.org/10.1130/G19702.1>
- Yan, Q., Kerty, R., Zhang, Z., & Wang, H. (2019). Evolution of tropical cyclone genesis regions during the Cenozoic era. *Nature Communications*, *10*, 3076. <https://doi.org/10.1038/s41467-019-11110-2>
- Yan, Q., Wei, T., Kerty, R. L., Kossin, J. P., Zhang, Z., & Wang, H. (2016). Enhanced intensity of global tropical cyclones during the mid-Pliocene warm period. *Proceedings of the National Academy of Sciences*, *113*, 12963–12967. <https://doi.org/10.1073/pnas.1608950113>
- Yan, Q., Wei, T., Zhang, Z., & Jiang, N. (2019). Orbitally induced variation of tropical cyclone genesis potential over the western North Pacific during the mid-Piacenzian warm period: A modeling perspective. *Paleoceanography and Paleoclimatology*, *34*, 902–916. <https://doi.org/10.1029/2018PA003535>
- Yang, Y., Piper, D. J. W., Normandeau, A., Zhou, L., Jia, J., Wang, Y. P., & Gao, S. (2022). A late Holocene shift of typhoon activity recorded by coastal sedimentary archives in eastern China. *Sedimentology*, *69*, 954–969. <https://doi.org/10.1111/sed.12934>
- Yu, H.-S., & Chou, Y.-W. (2001). Characteristics and development of the flexural forebulge and basal unconformity of Western Taiwan Foreland Basin. *Tectonophysics*, *333*, 277–291. [https://doi.org/10.1016/S0040-1951\(00\)00279-1](https://doi.org/10.1016/S0040-1951(00)00279-1)

- Zhao, Y., Zou, X., Gao, J., Wang, C., Li, Y., Yao, Y., Zhao, W., & Xu, M. (2018). Clay mineralogy and source-to-sink transport processes of Changjiang River sediments in the estuarine and inner shelf areas of the East China Sea. *Journal of Asian Earth Sciences*, 152, 91–102. <https://doi.org/10.1016/j.jseaes.2017.11.038>
- Zhao, Y., Zou, X., Liu, Q., Wang, C., Ge, C., & Xu, M. (2018). Clay mineralogy indicates the muddy sediment provenance in the estuarine-inner shelf of the East China Sea. *Journal of Asian Earth Sciences*, 152, 69–79. <https://doi.org/10.1016/j.jseaes.2017.11.036>

How to cite this article: Hsieh, A. I., Dashtgard, S. E., Wang, P.-L., Horng, C.-S., Su, C.-C., Lin, A. T., Vaucher, R., & Löwemark, L. (2023). Multi-proxy evidence for rapidly shifting sediment sources to the Taiwan Western Foreland Basin at the Miocene–Pliocene transition. *Basin Research*, 35, 932–948. <https://doi.org/10.1111/bre.12741>